Understanding mass fluvial erosion along a bank profile: Using PEEP technology for quantifying retreat lengths and identifying event timing

Athanasios N. (Thanos) Papanicolaou, Christopher G. Wilson, Achilles G. Tsakiris, Tommy E. Sutarto, Fabienne Bertrand, Massimo Rinaldi, Subhasish Dey, and Eddy Langendoen
Athanasios N. (Thanos) Papanicolaou*

Athanasios N. (Thanos) Papanicolaou*

- University of Tennessee, Civil & Environmental Eng

325 JD Tickle Bldg., 851 Neyland Dr.

Knoxville, Tennessee, United States

- tpapanic@utk.edu

Christopher G. Wilson

- University of Tennessee, Civil & Environmental Eng

325 JD Tickle Bldg., 851 Neyland Dr.

Knoxville, Tennessee, United States

- cgw24@utk.edu

Achilles G. Tsakiris

- University of Tennessee, Civil & Environmental Eng

325 JD Tickle Bldg., 851 Neyland Dr.

Knoxville, Tennessee, United States

- atsakiri@utk.edu

Tommy E. Sutarto

- Samarinda, Civil

120 Jakarta, Jakarta, Indonesia

- tommysutarto@gmail.com

This article has been accepted for publication and undergone full peer review but has not been through the copyediting, typesetting, pagination and proofreading process which may lead to differences between this version and the Version of Record. Please cite this article as doi: 10.1002/esp.4138

Fabienne Bertrand

- The University of Iowa, Civil Engineering

IIHR, Iowa City, Iowa City

- fabienne-bertrand@uiowa.edu

Massimo Rinaldi

- Dipartimento di Scienze della Terra,

Università di Firenze

Via La Pira, 4, Firenze, Italy

- mrinaldi@dicea.unifi.it

Subhasish Dey

- Indian Institute of Technology,

Department of Civil Engineering,

Kharagpur, West Bengal, India

- sdey@iitkgp.ac.in

Eddy Langendoen

- USDA, Agricultural Research Service

National Sedimentation Laboratory,

598 McElroy Drive, P.O. Box 1157

Oxford, Mississippi, United States

- eddy.langendoen@ars.usda.gov

Abstract

This study provides fundamental examination of mass fluvial erosion along a stream bank by identifying event timing, quantifying retreat lengths, and providing ranges of incipient shear stress for hydraulically driven erosion. Mass fluvial erosion is defined here as the detachment of thin soil layers or conglomerates from the bank face under higher hydraulic shear stresses relative to surface fluvial erosion, or the entrainment of individual grains or aggregates under lower hydraulic shear stresses.

We explore the relationship between the two regimes in a representative, U.S. Midwestern stream with semi-cohesive bank soils, namely Clear Creek, IA. Photo-Electronic Erosion Pins (PEEPs) provide, for the first time, in-situ measurements of mass fluvial erosion retreat lengths during a season. The PEEPs were installed at identical locations where surface fluvial erosion measurements exist for identifying the transition point between the two regimes. This transition is postulated to occur when the applied shear stress surpasses a second threshold, namely the critical shear stress for mass fluvial erosion.

We hypothesize that the regimes are intricately related and surface fluvial erosion can facilitate mass fluvial erosion. Selective entrainment of unbound/ exposed, mostly silt-sized particles at low shear stresses over sand-sized sediment can armor the bank surface, limiting the removal of the underlying soil. The armoring here is enhanced by cementation from the presence of optimal levels of sand and clay. Select studies show that fluvial erosion strength can increase several-fold when appropriate amounts of sand and clay are mixed and cement together. Hence, soil layers or conglomerates are entrained with higher flows.

The critical shear stress for mass fluvial erosion was found to be an order of magnitude higher than that of surface fluvial erosion, and proceeded with higher

(approximately 2-4 times) erodibility. The results were well represented by a mechanistic detachment model that captures the two regimes.

Keywords: mass fluvial erosion; PEEPs; erodibility; armoring; cementation; Clear Creek, IA

Introduction

Fluvial erosion in a stream channel involves the entrainment of bank soils into the flow resulting from an applied mean fluid shear stress, τ_w (Lawler *et al*., 1997; Millar and Quick, 1998; Huang *et al*., 2006). It is a low-to-intermediate magnitude, bank erosion process with a characteristic retreat scale during an event ranging from soil grains to conglomerates of grains (i.e., layers or clods). Additionally, fluvial erosion is a fairly high frequency, quasi-continuous process that potentially occurs along several segments of the channel reach (Rinaldi and Darby, 2008).

Fluvial erosion ensues when the τ_w over the bank face supersedes the resistance offered by the effective cohesion between soil grains (e.g., Partheniades, 1965; Kandiah, 1974; Millar and Quick, 1998; Righetti and Lucarelli, 2007). For semi-cohesive soils, resistance is dictated by different biogeochemical properties including electrostatic forces, pore water chemistry, clay mineralogy, and soil composition (Arulanandan, 1975; Commission of the European Community, 1993; van Klaveren and McCool, 1998). A surrogate measure of this resistance is the critical shear stress for fluvial erosion, τ_c (e.g., Sutarto *et al*., 2014; among others).

With fluvial entrainment, though, certain researchers have noticed a shift in erosion behavior above a shear stress value that is a multiple of τ_c. This shift is usually reflected with a change in the gradient for plots of erosion rate, E, vs. τ_w. This change in behavior has been observed in coastal erosion studies (e.g., Partheniades, 1965; Chapuis, 1986a; Mostafa *et al*., 2008; Winterwerp *et al*., 2012), as well as in upland soils and riverbed channels (Kamphuis *et al*., 1990; Wilson, 1993a,b; Vermeyen, 1995; Gaskin *et al*., 2003; Huang *et al*., 2006; Kothyari and Jain, 2008; Al-Madhhachi *et al*., 2014) where different phases or regimes of fluvial erosion have been defined. While the recognition of different regimes in fluvial entrainment across different disciplines is not new, the concept and mechanisms behind it for stream banks have not been investigated.

To help explain this potential shift in the behavior of fluvial erosion, postulates for the mechanisms behind and conditions under which surface and mass fluvial erosion occur are presented. Fluvial erosion is partitioned here into the different regimes of *surface fluvial erosion* and *mass fluvial erosion* (e.g., Winterwerp and van Kesteren, 2004) and the two regimes are deciphered by relating bank retreat length to hydraulic shear.

The grain-by-grain entrainment of the unbound or exposed particles characterizes surface fluvial erosion. As an analogy, a similar behavior has been noted with grain entrainment processes atop a riverbed, defined as stage I in sediment entrainment literature (e.g., Elhakeem *et al*., 2016; Papanicolaou and Tsakiris, 2017 - see Figure 5 therein, modified from Hassan *et al*., 2005).

The onset of surface fluvial erosion occurs at low mean shear stress values just exceeding τ_c, which is referred to hereafter as $\tau_{c,sf}$. In this case, the shear stress exceeds the van der Waal and Coulomb forces between soil grains leading to particle dislodgement referred to earlier (Partheniades, 2009). As surface fluvial erosion progresses, the available stock of easily erodible, finer soil particles on the bank face is depleted. The coarser, sand-

sized particles are, however, less susceptible to mean flow events and tend to remain on the bank surface. The inability of flows with low shear stress values to dislodge coarser particles has implications on bank surface structure and may be one of the triggering mechanisms for the potential shift observed in fluvial erosion behavior. The coarser particles, due to their predominant sizes, affect the bank surface structure by providing "hiding" for the incoming finer sized particles during a hydrograph (Motta *et al.*, 2012). Coarser particles "armor" the bank face, thus shielding the underlying finer size particles from entrainment (Reed *et al*., 1999; Le Hir *et al*., 2011).

Coarser particles available on the bank surface also work as "anchor" particles for the incoming finer size fraction. For instance, the clay minerals and calcium carbonates, like those found in loess-derived soils, can adhere to coarser sand particles leading to potential cementation if favorable proportions of sand and clay fractions are present (e.g., Krintzsky and Turnball, 1967). The finer particles tend to form a thin coat on the coarser particles linking them into thin layers of conglomerates, or clods (e.g., Trhlikova, 2013). The modification of the bank surface structure resulting from the armoring and adherence between coarse and fine fractions leading to thin layers of conglomerates, as well as consolidation and aging of the conglomerated material over time, collectively provide added resistance to the flow, leading to the genesis of the mass fluvial erosion regime (e.g., van Kessel and Blom, 1998; Reed *et al*., 1999; Le Hir *et al*., 2011; Winterwerp *et al*., 2012).

The transition from surface to mass fluvial erosion is postulated to occur when τ_w surpasses a second threshold value, namely the critical shear stress for mass fluvial erosion, $\tau_{c,mf}$ (e.g., Huang *et al*., 2006). Higher mean shear stress values above $\tau_{c,sf}$ are needed for the hydrodynamic forces to overcome the added resistance from armoring and cementation. Due to armoring and higher cementation, thin layers and clods, instead of just single particles, are entrained with the higher flows thus characterizing the mass fluvial erosion regime (e.g.,

UNESCO, 2013). By drawing an analogy for this new regime with sediment entrainment for riverbeds one could suggest that it corresponds to stage II, which is the intermediate stress regime for riverbed erosion (see Figure 5 in Papanicolaou and Tsakiris, 2017, modified from Hassan *et al*., 2005).

Understanding the transition from surface to mass fluvial erosion and quantifying mass fluvial erosion rates are crucial for constructing the spectrum of hydraulic conditions that bank erosion occurs. Few studies, thus far, consider the spectrum of hydraulic conditions extended to the two fluvial regimes. This knowledge is also important for developing watershed scale sediment budgets that account for eroded bank material contributions (Wilson *et al*., 2012).

Additionally, systematic measurements and data that relate bank retreat length (scaled from grain to clod size) to hydraulic shear for low-to-intermediate magnitude shear stresses are lacking. These data are valuable for evaluating process-based soil detachment models, which for bank fluvial erosion processes remain at their infancy. A handful of models (e.g., Wilson, 1993 a,b) can capture the presence of the two regimes for fluvial entrainment of semi-cohesive soils; however, the majority of these models have been calibrated based on data for rill flow detachment. Additionally, the mechanisms of armoring and cementation have not been fully considered in fluvial bank erosion processes (e.g., Winterwerp and van Kesteren, 2004; Huang *et al*., 2006; Kothyari and Jain, 2008).

In this study, we posit that the transition from surface to mass fluvial erosion is best represented by relating changes in bank retreat length to hydraulic shear. Figure 1 is a conceptual schematic that summarizes the two regimes of fluvial erosion for semi-cohesive banks. We hypothesize that the two regimes are intricately related and that surface fluvial erosion, as a precursor process, can create favorable conditions for mass fluvial erosion to

ensue at higher shear stresses, as explained earlier with the removal of the unbound surface grains.

Estimates of mass fluvial erosion rates using the relationship between bank retreat length and hydraulic shear through systematic measurements of $\tau_{c,mf}$ and the corresponding erodibility rate, M_{mf}, would therefore benefit from measuring devices that could detect bank retreat quasi-continuously to capture the initiation and magnitude of these erosion events (Lawler, 1992). Traditional measurement methods, such as channel cross-section surveys, terrestrial photogrammetry, and conventional erosion pins cannot capture the quasi-continuous nature of mass fluvial erosion for relating retreat lengths with specific hydrologic events (and corresponding stress levels), since they are conducted at discrete time instances (e.g., Chapuis, 1986b; Kamphuis *et al*., 1990). Other laboratory devices, like flumes and jet devices, have been successful at measuring surface fluvial erosion parameters (e.g., Al-Madhhachi *et al*., 2013; Sutarto *et al*., 2014; Khanal *et al*. 2016a,b), but they cannot reliably provide repeated measures of mass fluvial erosion due to the potential for sediment exhaustion occurring during the measurements (e.g., Chapuis, 1986a; Kamphuis *et al*., 1990; Gaskin *et al.*, 2003).

Past research (e.g., Lawler, 1991; 1992; 2005; 2008; Bertrand, 2010; Zaimes and Schultz, 2015) demonstrates the utility of Photo Electronic Erosion Pins (PEEPs) for measuring quasi-continuous retreat lengths in response to different hydrologic events. A PEEP is a simple, optoelectronic device containing a series of either photo-resistant or photo-voltaic cells (i.e., diodes) enclosed within a waterproofed, transparent, acrylic tube (Lawler, 1991; Rickly-Klausmeyer pers. comm.). The diodes are spaced at the centimeter scale making PEEPs ideal for acquiring retreat lengths corresponding to mass fluvial erosion of soil clods.

The important goals of this study are to define the spectrum of hydraulic conditions (i.e., the ranges of stress values) within which surface and mass fluvial erosion occur (see Figure 1) and support the postulate provided for potential mechanisms leading to the transition to mass fluvial erosion. Herein, PEEPs were used in a representative stream of the U.S. Midwest with semi-cohesive, loess-derived banks (Clear Creek, IA, USA) to identify the timing of mass fluvial erosion events and quantify in-situ retreat lengths along a bank profile (e.g., crest, midbank, and toe) in response to changes in flow depth and applied shear stress. This effort was complemented with a statistical treatment of the retreat length time series using Shewhart control charts to identify mass fluvial erosion events in terms of magnitude and their frequency of occurrence. The PEEP measurements were compared with conventional erosion pins which provide average retreat lengths over the monitoring period.

To demonstrate the transition point between the two regimes, we have compiled mass fluvial erosion parameters ($\tau_{c,mf}$ and M_{mf}) determined from the PEEPs with measurements of the corresponding surface fluvial erosion parameters using a conduit flume (Sutarto *et al*., 2014). Analysis of the complete dataset (namely surface and mass fluvial erosion measurements) from the same location in Clear Creek provides a unique opportunity to define the spectrum of hydraulic conditions (i.e., the range of stress values) within which surface and mass fluvial erosion occur. The data from the surface and mass fluvial erosion measurements are compared with the detachment model of Wilson (1993 a,b).

Site Selection

Clear Creek (Figure 2(a)) drains approximately 270 km^2 of mixed agricultural and urban lands to the Iowa and then Mississippi Rivers (Abaci and Papanicolaou, 2009). Bank retreat in Clear Creek has been exacerbated since intensive agriculture was introduced in the 1930s when farmers straightened the channel and cleared the vegetation along the floodplain (Langel, 1996; Landwehr and Rhoads, 2003; Knox, 2001; Rayburn and Schulte, 2009; Sutarto *et al*., 2014).

The monitoring site was selected near the mouth of Clear Creek, which experiences sustained higher flows facilitating bank erosion. Bank soils near the mouth of Clear Creek have, on average, more sand (53 ± 11%) and silt (39 ± 10%) than clay (8 ± 2%), especially at the upper parts of the bank profile, which are comprised of recently delivered sand sediment deposits from overbank flow events during late spring and early summer (Figure 2(b)). These conditions favor armoring of the finer fraction by the coarser material. The higher portion of sand and the adherence of clay to sand also lead to cementation and development of thin crusts of material. On average since 1960, there is at least 1 bankfull or greater flow in Clear Creek per year, with the range being between 0 and 7 times. The bank material at the crest is therefore less consolidated and aged than the material found at the lower bank with implications on the frequency that mass fluvial erosion occurs (see Figure 6 and corresponding discussion). This is reflected in the bulk density of the bank soils which increases moving down the bank profile as shown in Figure 3 (Sutarto *et al*., 2014).

Methodology

PEEP System Components and Operating Principle

To monitor mass fluvial erosion over a series of events, a PEEP sensor system (Figure 3) uses a solar panel that supplies power to both the PEEP and a data logger. The solar panel and data logger are mounted on a pole on the adjacent floodplain. Additionally, a "reference" PEEP is placed on top of the nearby floodplain and secured to a cement block. The fully exposed, reference PEEP provides the corresponding voltage outputs for the unobstructed ambient light conditions, V_{rp} (McDermott and Sherman, 2009).

The PEEP sensor (Figure 4) used in this study was produced by Rickly Hydrological Company and consists of 13 photo-resistance diodes in a series spaced 1.65-cm apart. PEEPs are inserted into the bank face and as the bank face erodes, more diodes are exposed to the sunlight. The resistance in each diode drops as it receives more sunlight, which increases the voltage output from the PEEP, V_{cs}, to the data logger sent along a connecting wire. The voltage outputs from the PEEP were logged at 15-sec intervals and averaged every 15 min in this study, similar to other PEEP studies (e.g., Couperthwaite *et al*., 1998; Mitchell *et al*., 2003; Horn and Lane, 2006; Lawler, 2008; McDermott and Sherman, 2009; Zaimes and Schultz, 2015).

The ratio, $R_r = V_{cs}/V_{rp}$, was related to the exposure length of the PEEP, L, through the calibration procedure described in the following section. The V_{rp} was used for normalizing the monitoring PEEP voltage outputs, V_{cs}, to account for minor fluctuations in sunlight intensity or from temporary shadows.

PEEP Calibration

The calibration of both the monitoring and reference PEEPs was conducted outdoors on the adjacent floodplain of the monitoring site at the mouth of Clear Creek on a sunny day (no clouds) around mid-day in May 2009. The PEEPs were placed horizontally on a fixed, level datum (i.e., a table with a levelling bubble). They were aligned perpendicular to the main stream flow direction to ensure nearly the same exposure and orientation with respect to the sunlight and bank face (Figure 4). The reference PEEP was fully exposed to the sunlight throughout the calibration. Black, light-tight sleeves initially covered all diodes of each monitoring PEEP (Figure 4). Every 4 min, these sleeves were pulled back 1.65 cm (i.e., distance equivalent to the diode spacing) which was manually confirmed with calipers. The normalized PEEP voltage ratios, R_r, were related to the measured exposure lengths of the PEEPs, L, using the following polynomial relationship (namely, the 2D National Institute of Standards & Technology (NIST)-Hahn Model):

$$L = \frac{(c_1 + c_2 R_r + c_3 {R_r}^2 + c_4 {R_r}^3)}{(1 + c_5 R_r + c_6 {R_r}^2 + c_7 {R_r}^3)} \quad (1)$$

The coefficients, $c_1 - c_7$, were determined for each PEEP using the open-source software at *http://zunzun.com/Equation/2/NIST/NIST%20Hahn/* (accessed March 2010).

Installation Procedure

Following calibration, the monitoring PEEPs were installed horizontally into the bank face through pre-augured holes (70 cm x 1.6 cm). The holes were carefully drilled to prevent "significant" disturbance to the surrounding bank face. Before inserting each PEEP into a hole, the cable at the back end of the sensor was attached to the side of the tube with sufficient slack to avoid snapping. The PEEPs were then inserted into the holes until all but the tips (~2.54 cm) of the PEEPs were exposed. The cables were then run back up the bank

face to the data logger through a garden hose for additional protection and fixed to the bank surface.

PEEPs were inserted at the crest, upper midbank, lower midbank, and toe of the southwest bank to capture retreat lengths along the profile (Figure 3). These positions were based on the relative consolidation of the bank profile (Sutarto *et al*., 2014). In conjunction with the PEEP installation, 45 traditional erosion pins made of 30-cm long galvanized steel nails were inserted into the bank face parallel to the water surface and in-line from the top of the bank to the toe at the same elevations of the PEEPs in a gridded pattern. Initially, the head of the nail was flush to the bank face. As the bank retreated, the exposed lengths of the nails were measured carefully using a measuring tape. The discrete readings from the erosion pins were averaged and compared against the PEEP measurements.

Near-bank Shear Stress Determination

Retreat lengths, ΔL, were considered to be the change in PEEP exposure lengths, L, resulting from a flow event. The retreat lengths were complemented with flow depth measurements, h, to determine the corresponding flow discharge for the triggering event. The flow depth was measured at 15-min intervals, similar to the PEEP logging rate, using the existing U.S. Geological Survey stream gauge (#05454300; Clear Creek near Coralville, IA) that was just downstream (~25 m) of the PEEPs. The discharge was determined using the established rating curve.

The flow depth measurements were used to generate a corresponding time series of the near-bank shear stress in the vicinity of the PEEPs. The τ_w exerted on each bank layer i along the bank profile (crest, upper midbank, lower midbank, and toe) corresponding to a PEEP location was defined as follows:

$$\tau_{wi} = \rho\, g\, R_i\, S \tag{2}$$

where ρ (kg/m^3) is the density of water; g (m/s^2) is the gravitational acceleration; R_i is the hydraulic radius corresponding to each layer; and S is the channel slope. R_i and S were obtained via cross-sectional surveys. Equation 2 provides a suitable approximation of the shear stress because Clear Creek lacks expansions/ contractions and compound cross-sections, since it has been channelized in most parts, thereby limiting any significant secondary currents (Papanicolaou *et al*., 2007). For context, bankfull flows at this site are 3.41 m or 56 m^3/s, which has a stress of ~20 Pa. The stress values have errors less than 6%, since they were derived from the stage-discharge measurements at the USGS gage site.

Uncorrected Exposure Lengths

As a preliminary step of the PEEP data analysis, the flow depth time series was examined to understand the dynamicity (i.e., timing and magnitude) of the various flow events. Figure 5(a) shows the h time series and the five high flow events during the monitoring period.

These hydrologic data were examined concomitantly with the voltage outputs from the monitoring PEEPs, V_{cs}, and reference PEEPs, V_{rp}. Figure 5(b) shows the V_{cs} for the PEEP at the bank crest with the dashed line and the corresponding V_{rp} with the solid line. At first glance, both V_{cs} and V_{rp} exhibited high variability within each day. V_{rp} ranged from about 0.5 to 1 with a regular pattern. The voltages of the reference PEEP, which was fully exposed at all times on the floodplain, were affected by changes in the ambient light intensity from the angle of the sun (this includes the low/no light conditions at dusk, dawn, and overnight) and clouds. The voltages of the monitoring PEEPs, V_{cs}, have wider ranges and exhibited irregular patterns as expected. The monitoring PEEPs, which were buried within the stream bank, were not only affected by the sun angle and clouds, but also by the bank angle, shadows from any vegetation, and of course, the exposure lengths due to bank retreat, thus causing the greater variability (Lawler, 2008).

A closer look at the voltage data from the monitoring PEEP highlights additional features. The circles in Figure 5(b) show periods when the V_{cs} dropped, which coincided with rises in flow depth for the different events. These drops were due to the collective effects of PEEP submergence and elevated turbidity in the stream, which caused attenuation in the light intensity and thereby affected PEEP output (e.g., McDermott and Sherman, 2009). Based on data for southeast Iowa streams, increases in Total Suspended Solids concentrations from 10 mg/l to 90 mg/l cause decreases in Secchi disk depths within the water column from 60 to 10 cm (Loperfido *et al*., 2009).

Additionally, Figure 5(b) shows periods when V_{cs} values approached V_{rp} values (see squares in the figure) following right after the high flow events on June 19 and August 27, 2009. The condition of $V_{cs} \approx V_{rp}$ indicates that the PEEP was almost fully exposed. To continue monitoring in this case, the PEEP was removed, the hole was re-augured, and the PEEP was reset into the stream bank so that only the tip was exposed.

One final feature of the PEEP voltage data was identified after determining exposure lengths with the calibration formula, Eq. 1. As seen in Figure 5(c), Eq.1 sometimes produced meaningless values that were either below zero or unreasonably large. This was especially apparent during dawn and dusk when the ambient light intensities were either too low or too bright due to the low-angled orientation of the sun yielding R_r values that were outside the calibration range of Eq. 1. It is important to remember that the PEEPs were calibrated for the "floodplain" ambient light intensity, which is not necessarily the ambient light intensity received by the PEEPs inserted in the bank face.

In summary, the above features suggest that the L from the calibration formula must first be "corrected" to account for the effects of variable light intensity, turbidity, and submergence, all of which can produce meaningless values if unaccounted. To address these

concerns, a data-processing procedure to quantify bank retreat and identify mass fluvial erosion events (Figure A1) was developed for this study and detailed below.

Corrected Exposure Lengths

The data processing procedure to quantify *L* using the PEEP voltages, V_{cs} and V_{rp}, consisted of three sequential stages, namely the "filtering", "correcting", and "smoothing" stages. Following the use of the calibration formula, the first step in the filtering stage was to remove voltages measured at night. Nighttime *L* can be considered meaningless, since PEEPs require light. The nighttime *L* values were essentially removed by setting them to zero. This step was repeated for the values obtained while the PEEPs were submerged (Figure 5(b)) and any other outlier values that were below zero or unreasonably large (Figure 5(c)).

In the "correcting" stage, the filtered *L* values were adjusted to account for the resetting of the PEEPs due to their near-full exposure. After resetting, the previous exposure lengths were added to the new measured exposure lengths. In this study, the crest, upper midbank, and lower midbank PEEPs were reset on July 7, 2009. The crest PEEP was reset again on September 11, 2009. Figure 5(d) as an example shows the *L* time series for the crest PEEP after the filtering and correcting stages were implemented. The daily peak *L* values were still highly variable.

To provide discrete, measureable *L* readings in between hydrologic events, a moving average (e.g., Whittaker and Robinson, 1967) was performed in the "smoothing" stage. In this case, the moving average removes minor signal variations from short-term fluctuation in ambient light conditions.

$$Moving\ Average = \frac{(L_t + L_{t-1} + \ldots + L_{t-(n-1)})}{(n)} \quad (3)$$

where *L* is the PEEP exposure length at time *t* and *n* is the number of equally spaced, 15-min intervals of the PEEP measurements in the respective time span.

Moving average intervals from 1 to 24 hr were examined based on the most prominent erosion-related events for the study site (Bertrand, 2010). An 8-hr moving average was determined to be the most effective as lesser intervals did not remove enough of the variability, while larger intervals provided similar results. The moving-average effectively produced more stable daily peaks and more emergent erosion-related increases (dashed black line in Figure 5(e)) comparatively to the un-smoothed L (Figure 5(d)).

The second smoothing step involved setting the L to the maximum value of the time series between erosion events (solid grey line in Figure 5(e)). This was based on the consideration that the maximum PEEP voltage output provided the closest "true" estimate of L (e.g., Lawler *et al*., 2001; McDermott and Sherman, 2009) as lesser values would result from lower ambient light conditions. This consideration is reasonable at this stage of data processing as the "false" peak values have already been removed.

The final smoothing step was based on the supposition that any measured L value less than the 1.65-cm spacing between diodes, or was not a multiple of this cell spacing, was not considered. This rounding would constitute the error in the PEEP measurements. This smaller degree of erosion less than 1.65 cm could be attributed to just surface fluvial erosion occurring or attributed to the misalignment of the PEEPs from the horizontal position, poor water transparency, or the presence of scattered clouds. Vibration caused by the potential spiral motion induced by the flow must also be considered as a potential source of error. The L values were rounded to the cell spacing length or closest multiple as seen with the stair-cased solid line in Figure 5(e) and represents the best estimate of exposure length. An increase in this estimated L (or ΔL) signifies the occurrence of a new mass fluvial erosion event.

Results and Discussion

The results of this study focus on the hydraulic conditions under which mass fluvial erosion occurs and the corresponding rates of mass fluvial erosion; further, the surface fluvial erosion results (from Sutarto *et al.*, 2014) from the identical locations in Clear Creek are appended to provide the entire spectrum of hydraulic conditions for fluvial erosion.

The results are organized as follows. First, the time series data obtained with the PEEPs are provided, followed by a statistical analysis (namely Shewhart control charts) in order to identify whether the exposure lengths following a storm event were significantly different from the mean exposure lengths prior to the event, thus signifying mass fluvial erosion.

Second, pairs of corresponding applied shear stress and PEEP-derived mass fluvial erosion rate are plotted (similar to Figure 1) to determine the mass fluvial erosion parameters of $\tau_{c,mf}$ and M_{mf}. These data are plotted together with existing pairs of applied shear stress and surface fluvial erosion rate from the same locations as the PEEP measurements in Clear Creek (Sutarto *et al*., 2014) to provide the spectrum of stresses for which hydraulically driven erosion occurs either as surface or mass fluvial erosion. The analysis is also complemented with a comparison to a mechanistic detachment model (Wilson, 1993a,b).

Magnitude and Frequency of Mass Fluvial Erosion

Figure 6 relates the time series of flow depth, h, to the L time series determined using the procedure outlined in Figure A1 for the PEEPs installed at the crest (Figure 6(b)), upper midbank (Figure 6(c)), lower midbank (Figure 6(d)), and toe (Figure 6(e)) for the period between June 1 and December 1, 2009.

The bank retreat lengths at each PEEP location on an event basis were of a similar range, between 1.6 and 13.2 cm. The retreat lengths are seen as the staircase jumps in the solid grey lines in Figure 6. The similar ranges of mass erosion per event suggest that all locations experience armoring and cementation, which were confirmed visually (Figures 3 and 7, respectively) and through soil composition testing (Sutarto *et al*., 2014).

It is also important to note that the biggest step changes occurred early in the season (i.e., during the June 19, 2009 storm event), when the soils had less vegetation coverage. Cumulatively, the crest therefore had the highest bank retreat of 41 cm over the monitoring period, while the upper and lower midbank locations had 29.6 and 27.6 cm, respectively, and the toe had only 6.6 cm.

Table 1 provides a summary of the bank retreat measurements and includes measurements from the PEEPs and traditional erosion pins. The readings from the PEEPs were compared to those of the nearest pins. Overall close agreement was observed between the datasets confirming the results by the PEEPs. A t-test between the PEEP and pin datasets showed that the values were not statistically different ($p = 0.98$). The retreat measurements from the PEEPs located at the crest, upper and lower midbank were all higher than the corresponding pin measurements, while the ΔL from the PEEP located at toe was lower than the corresponding traditional measurements.

Table 2 describes potential sources of error between the PEEPs and pins. The bank soils near the crest are less consolidated than the locations lower in the bank profile (see Figure 10 from Sutarto *et al*., 2014) producing a higher likelihood for the PEEP to spin slightly out of the augured hole, suggesting a higher retreat length. In addition, the larger exposure lengths of the PEEPs potentially triggered higher disturbance by obstructing more of the flow, further supporting the need to re-set the PEEPs periodically.

While the bank retreat lengths at each PEEP location on an event basis were similar, the frequency of mass erosion varied along the bank profile. The crest location experienced the most number of mass fluvial erosion events due in part to its lower overall consolidation and soil age (Sutarto *et al.*, 2014), which make it more prone to mass fluvial erosion. Newly deposited sediment at the crest has less time to cement and consolidate in comparison to soil at the lower sections.

Shewhart control charts were constructed using the PEEP exposure lengths per location (Figure 8). The construction of the Shewhart control charts was used as a means to confirm statistically that the retreat lengths shown in Figure 6 correspond to mass fluvial erosion. The daily maximum values for the L time series were compared with the mean and upper control limit, represented by the solid and dashed grey lines in Figure 8. The upper control limit is the mean value plus a baseline variation of three times the standard error (Chatfield, 1984; Vardeman and Jobe, 1999). The standard error was determined as the standard deviation divided by the square root of the number of measurements. The lower control limits are not shown as the retreat lengths far exceeded them (and to avoid figure overcrowding).

The exposure lengths after the two largest events on June 19 and August 27, 2009 exceeded the upper control limit, and for the other events, the values approached it or slightly surpassed it.. Thus, they were significantly different than the mean exposure lengths prior to the storm events and this was deemed as a sign of mass fluvial erosion.

Erodibility

The bank retreat lengths determined from each PEEP were integrated over the total bank height for a 1-m wide section of the bank face and were used to quantify the erodibility, M_{mf}, of the bank soil, in kg/s as follows (Palmer *et al*., 2014):

$$M_{mf} = \frac{mass\ of\ erosion}{time\ of\ erosion} = H_{bank} \times W \times \left(\frac{\Delta L}{\Delta T}\right) \times \rho_{bulk} \quad (4)$$

where H_{bank} (m) is the bank height; W (m) is the 1-m wide section of the bank face; ΔL (m) is the bank retreat integrated over the height of the bank determined using the PEEPs (Table 3); ΔT (s) is the time of mass fluvial erosion (Table 3); and ρ_{bulk} (kg/m^3) is the bulk density of bank soil.

The ΔL values for the June 19, 2009 flow event, shown in Figure 6, are used to demonstrate the quantification of M_{mf} for the bank soil, as the largest retreat was measured at all four PEEP locations during this event. The integrated retreat length over the bank height (3.46 m) with a 1-m width was 9.40 cm.

Figure 9 shows the time series of τ_w for the PEEPs during the June 19, 2009 event and the procedure used to estimate M_{mf}. The time of mass fluvial erosion, ΔT, was defined as the time of the initial increase (surge) in the water depth or when the applied shear stress, τ_w, increased rapidly for the first time. It has been suggested in the literature that the initial "punch" to the bank face from stress values over the threshold value triggers erosion (Julian and Torres, 2006). The period of time when each location on the bank experienced stresses higher than $\tau_{c,m}$ are represented in Figure 9 with grey bars. The earliest rapid increase of τ_w is highlighted by the circles in Figure 9. The length of time for this initial increase, or ΔT, (Table 3) was determined using the change in gradient (Figure 9(e)). For example, at the crest of the bank, the initial increase lasted 1800 s, or 0.5 hour, which is represented with the first rise of the line.

As a result, the M_{mf} for this event was found to be 0.332 kg/s based on Eq. 4. This event, which was the first one monitored, had the highest erodibility. Because it occurred early in the season, the soil had less vegetation coverage and was more prone to the higher erosion rates.

Critical Shear Stress for Mass Fluvial Erosion

The ΔL time series data were plotted with the corresponding τ_w for the different locations where the PEEPs were installed (Figure 10). These plots were used to identify pairs of corresponding applied shear stress, τ_w, and erosion rate, E, for each event. These pairs were used to determine $\tau_{c,mf}$ by plotting them in Figure 11. The erosion rate (kg/m^2/s) for each location was determined using the retreat rate ($\Delta L / \Delta T$) obtained from the PEEPs and the bulk density for a 1-m width.

Additionally, the results from Sutarto *et al*. (2014), which provided the critical shear stress for surface fluvial erosion, $\tau_{c,sf}$, of bank soils from the same locations as the PEEPs were also plotted. The corresponding $\tau_{c,sf}$ for these data average 1.8 ± 0.4 Pa. The maximum error for these tests was 12%, with the average error being below 6% (Sutarto *et al*., 2014).

To explain the connection between surface and mass fluvial erosion in Clear Creek, the following relationships between the data sets were explored: single linear, single non-linear, and piecewise linear. Single-line fits (linear or non-linear) suggest a gradual transition to higher erosion rates and no change in mechanism. The piecewise fit suggests a clearer threshold between regimes where fluvial erosion mechanisms shift allowing for the removal of soil layers and clods to overshadow the removal of individual particles.

The piecewise line segments were found to fit better the data than both the single linear fit and single non-linear fit using a weighted regression, which is seen through the respective R^2 values of 0.81, 0.37, and 0.52 (Table 4). The piecewise fit was significantly different using an F-test and a 10% confidence level from the single line fits. Other studies (e.g., Lyle and Smerdon, 1965; Parker *et al*., 1995; Zhu *et al*., 1995) have used split linear relations between erosion and applied shear stress, one for low shear stresses and one for higher shear stresses. The $\tau_{c,mf}$ is equal to 15.78 Pa for this bank soil, as defined using a

piecewise regression (Figure 11(b)). To put this in a context, this shear stress level corresponds to about a 3-m depth, just shy of bankfull conditions, and a flow rate of 46 m^3/s.

We suggest that in Clear Creek at low mean shear stress levels just above $\tau_{c,sf}$, selective entrainment of the unbound and exposed, mostly silt-size, particles coarsens the bank face thus increasing armoring of the surface (e.g., Figure 7). The coarsening is enhanced by sand deposits delivered during high flows (e.g., Figure 2(b)).

The mixture of sand and loess-derived clay that remains on the bank face are at optimal levels for cementation (e.g., Panagiotopoulos *et al*., 1997; van Ledden *et al*., 2004; Le Hir *et al*., 2008). Select studies have shown that fluvial erosion strength can increase several-fold when appropriate amounts of sand (~60%) and clay (~10%) are mixed and cement together, enhancing the armoring (Williamson and Ockenden, 1993; Torfs, 1995; Berlamont and Torfs, 1995; van Ledden *et al*., 2004).

Additional analysis of index properties by Sutarto *et al*. (2014) confirms the Clear Creek bank soils as having a critical level of clay with sand that, when coupled with consolidation, leads to cementation (e.g., Panagiotopoulos *et al*., 1997; van Ledden *et al*., 2004; Le Hir *et al*., 2008). It is likely that cementation in the Clear Creek facilitates the removal of soil layers and clods under hydraulic shear stresses greater than $\tau_{c,mf}$, once the individual, unbound/ exposed, particles at the surface are exhausted by surface fluvial erosion. In Figure 11(b), we suggest that the change in slope (seen with the solid black line) represents the threshold breakpoint between surface and mass fluvial erosion (Vermeyen, 1995; Huang *et al*., 2006).

To further illustrate the need for representing fluvial erosion in terms of two separate regimes, a low mean stress regime for surface fluvial erosion and a high mean stress regime for mass fluvial erosion, we applied our stress data to an established non-linear entrainment model by Wilson (1993a,b), which has been adjusted by Al-Madhhachi *et al*., (2014) and

applied to stream banks by Khanal *et al*., (2016b). The model captures mechanistically the drag and lift forces acting on a soil grain, as well as some of the sources of resistance.

$$\varepsilon_r = b_0 \times \sqrt{\tau_w} \times \left\{1 - e^{\left[-e^{\left(3-\frac{b_1}{\tau_w}\right)}\right]}\right\} \quad (5)$$

where ε_r is the total erosion rate and b_0 and b_1 are dimensional parameters that reflect properties of the sediment (see Wilson, 1993a,b for further description). In the above equation, τ_w represents the average shear stress exerted on the bank surface. In practice, Eq. (5) is fit to the measured E and τ_w data by adjusting the coefficients b_0 and b_1. However, in this case the coefficients b_0 and b_1 were determined using the supplied model equations (namely equations 5a and 5b on p. 1116 in Wilson, 1993a,b).

Initially, a single set of coefficients for b_0 and b_1 was used to represent the whole range of stress values seen in Figure 11(a). This case is called the "single non-linear fit" and is represented with the dashed line. We were unable to capture well both the high and low mean stress data series, as seen with part of the dashed line plotting on the x-axis.

However, a better fit was obtained when representative values for the coefficients b_0 and b_1 were used for the two regimes (seen with the dashed line in Figure 11(b) and summarized in the enclosed table). These values were obtained by using τ_w values corresponding to the low-mean (flume) and high-mean (PEEP) stress data series, as well as by adjusting the K_e parameter in the Wilson model that considers the exposure of the particles and represents here changes in the surface structure of the bank face (Wilson 1993a,b; Al-Madhhachi *et al*., 2014; Khanal *et al*., 2016b). In the low stress series, which capture the surface fluvial regime, we see an increase as unbound/ exposed particles begin to erode but then the trend flattens as the available stock is exhausted. A steeper increase is seen at the higher stresses (corresponding to mass fluvial erosion) as cemented layers and clods start to erode. The comparison between the Wilson (1993a,b) model and the piecewise results from

Figure 11(b) highlights the importance of the mechanisms of armoring and cementation. Like in the case of piecewise regression where line segments adequately represent the two regimes the Wilson model better represents the two regimes when representative coefficient values for the two regimes are employed.

Conclusion

The contributions of this research span across the spectrum of fluvial erosion. An extensive literature review on this topic revealed two major shortcomings: (1) the realization that only a small number of fluvial geomorphology studies have considered the role of mass fluvial erosion; and (2) there exists a lack of the mechanisms that lead to the occurrence of mass fluvial erosion.

This study provides unique data distinguishing the breakpoint between mass fluvial erosion and surface fluvial erosion and is a first attempt to relate the different length scales between surface and mass fluvial erosion with the shear stress ranges for the two regimes. Both regimes are hydraulically driven and in this case, mass fluvial erosion follows surface fluvial erosion as it results from a higher shear stress and exhibited accelerated erodibility (i.e., M_{mf}).

It was found that the $\tau_{c,mf}$ was an order of magnitude higher than the measured $\tau_{c,sf}$ using a conduit flume and soil samples from the same location. The erodibility rates M_{mf} were about 2 to 4 times higher than M_{sf}. This agrees with the limited number of reported studies for mass fluvial erosion (Chapuis, 1986a; Kamphuis *et al*., 1990; Vermeyen, 1995; Winterwerp and van Kesteren, 2004). Hence, mass fluvial erosion should neither be ignored nor assumed to be affected by the same mechanisms as surface fluvial erosion. While both regimes are hydrodynamically driven in the case of mass fluvial erosion cementation and consolidation were suggested as mechanisms that can affect the retreat length and frequency

of occurrence of mass fluvial erosion, although further understanding is required (see Figure 6). This type of information is lacking in the bank erosion literature and is crucial for identifying more definitively the erosion responses of bank soils to different hydraulic shear stresses within a wide range of high-flow events.

The findings in this study are made possible by methodological advancements towards estimating $\tau_{c,mf}$. Current laboratory methods used to estimate $\tau_{c,sf}$ cannot provide accurate, repeatable measures of the critical shear stress for mass fluvial erosion, since sediment exhaustion during the laboratory runs is more likely.

Based on that realization, PEEPs were used, for the first time, to provide unique in-situ measurements of the $\tau_{c,m}$ and hence insight into the mass fluvial erosion retreat lengths during a season. Mass fluvial erosion estimations are greatly benefited from just the PEEPs, because they provide semi-continuous observations of retreat length magnitude and timing. Additionally, the PEEPs provide measurements on the cm scale, which corresponds with the characteristic clod length scale for mass fluvial erosion. A unique and systematic data processing routine (e.g., filtering, correcting and smoothing) was developed herein to facilitate the use of the PEEP measurements that removed the effects of ambient light changes due to solar orientation and other factors causing low light intensities (e.g., turbidity).

Finally, the necessary tools (like the PEEPs) now exist to define further the breakpoints between the different regimes of fluvial erosion, yet it is difficult to distinguish total contributions from surface fluvial erosion and mass fluvial erosion using the PEEPs, especially while the event is occurring. The interaction of the different regimes can be difficult to evaluate along a stream reach, as they most likely act in conjunction, particularly in the middle and lower stream reaches (Papanicolaou *et al*., 2006). To capture the

interaction between the regimes, it is necessary to investigate bank changes at the intra-event scale.

More research is however needed that focuses on the systematic preprocessing and post-processing of the PEEP data considering the fact that PEEPs can reliably reproduce a bank profile prior to and after the onset of a mass fluvial erosion event. Future research efforts should explore different ways to calibrate the PEEPs at the same levels of the bank face, and the role of vibrations or spinning of the PEEPs due to the flow, as well as the effects of total suspended sediment, poor water transparency and the presence of scattered clouds as it relates to the ambient light conditions. Note that the PEEPs were calibrated with the diodes facing skyward, being perpendicular to the light. Vibrations and rotation of the PEEPs can result in a change in the orientation of the diodes, which is difficult to account for during the three-stage preprocessing process (Figure A1).

Future work must also consider the effects of freeze-thaw cycles on surface and mass fluvial erosion strength. This need is prevalent in the U.S. Midwest where freeze-thaw cycles are prevalent throughout parts of the year. More light must be shed on the parameterization of the $\tau_{c,mf}$ and methods used for its estimation. It remains difficult to compare $\tau_{c,mf}$ values across studies due to the variety of testing devices.

In summary, the important contributions of this study are twofold. Using the PEEPs, erodibility rates and retreat lengths for mass fluvial erosion were provided in-situ for the first time based on a wide range of flow conditions. The potential mechanisms leading to mass fluvial erosion were presented although further understanding is required. Second, with state-of-the-art tools like the PEEPs and the conduit flume (see Sutarto *et al*., 2014), the distinction between surface and mass fluvial erosion with values for the incipient shear stresses was identified with the help from the linear piecewise regression for data points selected from identical locations. This more accurate quantification of the bank erosion regimes will have

ramifications to stream restoration work, bank stability analysis, as well as sediment source identification studies.

Acknowledgements

This research is partially supported by the NSF Grant # EAR-1331906 for the Critical Zone Observatory for Intensively Managed Landscapes (IML-CZO), a multi-institutional collaborative effort. The study stems from seed funding through the University of Iowa Obermann Center of Excellence Research Award for Research Issues for Riverine Bank Stability Analysis in the 21st Century (2005-2006) that the first author and Professors Dey and Rinaldi received. A grant from Iowa Department of Transportation supplemented further analysis at the study location. The authors are highly indebted to engineer David Claman, who has heavily influenced this work, its quality, and course with his comments.

References

Abaci O, Papanicolaou AN. 2009. Long-term effects of management practices on water-driven soil erosion in an intense agricultural sub-watershed: Monitoring and modeling. *Hydrological Processes* **23**(19): 2818-2837.

Al-Madhhachi AT, Fox GA, Hanson GJ, Tyagi AK, Bulut. R, 2014. Mechanistic detachment rate model to predict soil erodibility due to fluvial and seepage forces. *Journal of Hydraulic Engineering* **140**(5): 04014010.

Al-Madhhachi AT, Hanson GJ, Fox GA, Tyagi AK, Bulut R. 2013. Measuring soil erodibility using a laboratory "mini" JET. *Transactions of the ASABE* **56**(3): 901-910.

Arulanandan K. 1975. Fundamental aspects of erosion of cohesive soils. *Journal of the Hydraulics Division* **101**(NHY5): 635-639.

Berlamont JE, Torfs HM. 1996. Modeling (partly) cohesive sediment transport in sewer systems. *Water Science & Technology* **33**(9): 171-178.

Bertrand F. 2010. *Fluvial Erosion Measurements of Streambank Using Photo-Electronic Erosion Pins (PEEP)*. Master thesis, University of Iowa: Iowa City, IA.

Chapuis RP. 1986a. Use of rotational erosion device on cohesive soils. *Transportation Research Record N1089, Geotechnical Engineering*. Transportation Research Board: Washington DC; 23-28.

Chapuis RP. 1986b. Quantitative measurement of the scour resistance of natural solid clays. *Canadian Geotechnical Journal* **23**(2): 132-141.

Chatfield C. 1984. *The Analysis of Time Series: An Introduction*. Chapman & Hall: London, UK.

Commission of the European Community. 1993. Coastal morpho-dynamics: On the methodology and accuracy of measuring physic-chemical properties to characterize cohesive sediments. EC MAST-I Report: Amsterdam, Netherlands.

Couperthwaite JS, Mitchell SB, West JR, Lawler DM. 1998. Cohesive sediment dynamics on an inter-tidal bank on the Tidal Trent, UK. *Marine Pollution Bulletin* **37**(3-7): 144-154.

Elhakeem M., Papanicolaou AN, Tsakiris AG. 2016. A probabilistic model for sediment entrainment: The role of bed irregularity. *International Journal of Sediment Research* DOI: 10.1016/j.ijsrc.2016.11.001i.

Gaskin SJ, Pieterse J, Al-Shafie A, Lepage S. 2003. Erosion of undisturbed clay samples from the banks of the St. Lawrence River. *Canadian Journal of Civil Engineering* **30**: 585-595.

Hassan MA, Church M, Lisle TE, Brardinoni F, Benda L, Grant GE. 2005. Sediment transport and channel morphology of small, forested streams. *Journal of the American Water Resources Association* **41**(4): 853-876.

Horn DP, Lane SPH. 2006. Measurement of high-frequency bed level changes in the swash zone using Photo-Electronic Erosion Pins (PEEPs). *Proceedings of the 30th International Conference on Coastal Engineering*: San Diego, CA; 2591-2603.

Huang J, Hilldale RC, Greimann BP. 2006. Cohesive sediment transport. In: Yang CT(ed.). *Erosion and Sedimentation Manual*. U.S. Department of Interior, Bureau of Reclamation, Technical Service Center: Denver, CO; 4.1-4.54.

Julian JP, Torres R. 2006. Hydraulic erosion of cohesive riverbanks. *Geomorphology* **76**(1-2): 193-206.

Kamphuis JW, Gaskin PN, Hoogendoorn E. 1990. Erosion test on four intact Ontario clays. *Canadian Geotechnical Journal* **27**: 692-696.

Kandiah A. 1974. Fundamental aspects of surface fluvial erosion of cohesive soils. Ph.D. dissertation, University of California: Davis, CA.

Khanal A, Fox GA, Al-Madhhachi AT. 2016a. Variability of erodibility parameters from laboratory mini jet erosion tests. *Journal of Hydrologic Engineering* doi:10.1061/(ASCE)HE.1943-5548.0001404.

Khanal A, Klayon KR, Fox GA, Daly ER. 2016b. Comparison of linear and nonlinear models for cohesive sediment detachment: Rill erosion, hole erosion test, and streambank erosion studies. *Journal of Hydraulic Engineering* doi:10.1061/(ASCE)HY.1943-7900.0001147.

Knox JC. 2001. Agricultural influence on landscape sensitivity in the Upper Mississippi River Valley. *Catena* **42**: 193-224.

Krintzsky EL, Turnbull WJ. 1967. Loess deposits of Mississippi. *Geological Society of America Special Papers* **94**: 1-62.

Kothyari UC, Jain, RK. 2008. Influence of cohesive on the incipient motion condition of sediment mixtures. *Water Resources Research* **44**(4): W04410.

Landwehr K, Rhoads BL. 2003. Depositional response of a headwater stream to channelization, East Central Illinois, USA. *River Research and Application* **19**: 77-100.

Langel RJ. 1996. An Evaluation of Stream Bank Stabilization Utilizing Deep-planted Cuttings, Clear Creek, Johnson County, Iowa. M.S. thesis, University of Iowa: Iowa City, IA.

Lawler DM. 1991. A new technique for the automatic monitoring of erosion and deposition rates. *Water Resources Research* **27**(8): 2125-2128.

Lawler DM. 1992. Design and installation of a novel automatic erosion monitoring system. *Earth Surface Processes and Landforms* **17**: 455-463.

Lawler DM. 2005. The importance of high-resolution monitoring in erosion and deposition dynamics studies: Examples from estuarine and fluvial systems. *Geomorphology* **64**: 1-23.

Lawler DM. 2008. Advances in the continuous monitoring of erosion and deposition dynamics: Developments and applications of the new PEEP-3T system. *Geomorphology* **93**: 17-39.

Lawler DM, Thorne CR, Hooke JM. 1997. Bank erosion and instability. In Thorne CR, Hey RD, Newson MD (eds). *Applied Fluvial Geomorphology for River Engineering and Management*. John Wiley & Sons, Chichester, UK. pp. 137-172.

Lawler DM, West JR, Couperthwaite JS, Mitchell SB. 2001. Application of a novel automatic erosion and deposition monitoring system at a channel bank site on the tidal River Trent, U.K. Estuarine. *Coastal and Shelf Science* **53**: 237-247.

Le Hir P, Cayocca F, Waeles B. 2011. Dynamics of sand and mud mixtures: A multiprocess-based modelling strategy. *Continental Shelf Research* **31**(10): S135-S149.

Loperfido JV, Just CL, Schnoor JL. 2009. High-frequency diel dissolved oxygen stream data modeled for variable temperature and scale. *Journal of Environmental Engineering* **135**(12): 1250-1256.

Lyle WM, Smerdon ET. 1965. Relation of compaction and other soil properties to erosion resistance of soils. *Transactions of the American Society of Agricultural Engineers* **8**: 419-422.

McDermott JP, Sherman DJ. 2009. Using photo-electronic erosion pins for measuring bed elevation changes in the swash zone. *Journal of Coastal Research* **25**(3): 788-792.

Millar RG, Quick MC. 1998. Stable width and depth of gravel-bed rivers with cohesive banks. *Journal of Hydraulic Engineering* **124**(10): 1005-1013.

Mitchell SB, Couperthwaite JS, West JR, Lawler DM. 2003. Measuring sediment exchange rates on an intertidal bank at Blacktoft, Humber Estuary, UK. *The Science of the Total Environment* **314-316**: 535-549.

Mostafa TS, Imran J, Chaudhry MH, Kahn IB. 2008. Erosion resistance of cohesive soils. *Journal of Hydraulic Research* **46**(6): 777-787.

Motta D, Abad JD, Langendoen EJ, García MH. 2012. The effects of floodplain soil heterogeneity on meander planform shape. *Water Resources Research* **48**: W09518, doi:10.1029/2011WR011601.

Palmer JA, Schilling KE, Isenhart TM, Schultz RC, Tomer MD. 2014. Streambank erosion rates and loads within a single watershed: Bridging the gap between temporal and spatial scales. *Geomorphology* **209**: 66-78.

Papanicolaou AN, Dey S, Rinaldi M, Mazumdar A. 2006. Research issues for riverine bank stability analysis in the 21st century. Final report to the Obermann Center, University of Iowa, Iowa City, USA.

Papanicolaou AN, Elhakeem M, Hilldale R. 2007. Secondary current effects on cohesive river bank erosion. *Water Resources Research* **43**(W12418), doi: 10.1029/ 2006WR005763.

Papanicolaou AN, Tsakiris AG. 2017. Boulder effects on turbulence and bedload transport. Gravel Bed Rivers 8. In Press.

Parker DB, Michel TG, Smith JL. 1995. Compaction and water velocity effects on soil erosion in shallow flow. *Journal of Irrigation and Drainage Engineering* **121**(2): 170-178.

Partheniades E. 1965. Erosion and deposition of cohesive soils. *Journal of Hydraulics Division* **91**(HY1):105-138.

Partheniades E. 2009. *Cohesive Sediment in Open Channels*. Butterworth-Heinemann Publishers. 384pp.

Panagiotopoulos I, Voulgaris G, Collins MB. 1997. The influence of clay on the threshold of movement on fine sandy bed. *Coastal Engineering* **32**: 19-43.

Rayburn AR, Schulte LA. 2009. Landscape change in an agricultural watershed in the US Midwest. *Landscape and Urban Planning* **93**(2): 132-141.

Reed CW, Niedoroda AW, Swift DJ. 1999. Modeling sediment entrainment and transport processes limited by bed armoring. *Marine Geology* **154**(1): 143-154.

Righetti M, Lucarelli C. 2007. May the Shields theory be extended to cohesive and adhesive benthic sediments?. *Journal of Geophysical Research* **112**: doi: 10.1029/2006JC003669.

Rinaldi M, Darby SE. 2008. Modeling river-bank-erosion processes and mass failure mechanisms: Progress towards fully coupled simulations. In: Habersack H, Piegay H, Rinaldi M (eds.). *Gravel-bed Rivers VI: From Process Understanding to River Restoration*. Elsevier, Amsterdam, Netherlands. pp. 213-239.

Sutarto TE, Papanicolaou AN, Wilson CG, Langendoen EJ. 2014. Stability analysis of semi-cohesive streambanks with CONCEPTS: Coupling field and laboratory investigations to quantify the onset of fluvial erosion and mass failure. *Journal of Hydraulic Engineering* **140**(9): 04014041, doi: 10.1061/(ASCE)HY.1943-7900.0000899.

Torfs H. 1995. *Erosion of Mud/Sand Mixtures*. Ph.D. Thesis, Katholieke Universiteit Leuven.

Trhlikova J. 2013. *Mechanical Behavior of Cemented Fine-Grained Soils: Simulation of Undisturbed Samples*. Ph.D. Thesis, Charles University in Prague.

UNESCO. 2013. *Soil Erosion and Sediment Production on Watershed Landscapes: Processes and Control*. Ffolliott PF, Neary DG, Brooks KN, Tapia RP, Chevesich PG. Documentos Técnicos del PHI-LAC, N#32.

van Kessel T, Blom C. 1998. Rheology of cohesive sediments: comparison between a natural and an artificial mud. *Journal of Hydraulic Research* **36**(4): 591-612.

van Klaveren RW, McCool DK. 1998. Erodibility and critical shear of a previously frozen soil. *Transactions of the American Society of Agricultural Engineers* **41**(5): 1315-1321.

van Ledden M, van Kesteren WGM, Winterwerp JC. 2004. A conceptual framework for the erosion behavior of sand-mud mixtures. *Continental Shelf Research* **24**(1): 1-11.

Vardeman SB, Jobe JM. 1999. *Statistical Quality Assurance Methods for Engineers*. John Wiley & Sons, New York, NY. pp. 561.

Vermeyen T. 1995. Erosion and depositional characteristics of cohesive sediments found in Elephant Butte Reservoir, New Mexico. *Technical Report R-95-15*, Water Resources Services, Technical Service Center, U.S. Bureau of Reclamation. Denver, USA.

Whittaker ET, Robinson G. 1967. *The Calculus of Observations: A Treatise on Numerical Mathematics*, 4th ed.: New York, NY; 285-316.

Williamson H, Ockenden M. 1993. Laboratory and field investigations of mud and sand mixtures. *Advances in Hydro-Science and Engineering* **1**: 622-629.

Wilson BN. 1993a. Development of a fundamentally based detachment model. *Transactions of the American Society of Agricultural Engineers* **36**(4): 1105-1114.

Wilson BN. 1993b. Evaluation of a fundamentally based detachment model. *Transactions of the American Society of Agricultural Engineers* **36**(4): 1115-1122.

Wilson CG, Papanicolaou AN, Denn KD. 2012. Quantifying and partitioning fine sediment loads in an intensively agricultural headwater system. *Journal of Soils and Sediments* **12**(6): 966-981.

Winterwerp JC, van Kesteren WGM. 2004. *Introduction to the Physics of Cohesive Sediment in the Marine Environment*. Elsevier: New York, NY; 343-379.

Winterwerp JC, van Kesteren WGM, van Prooijen B, Jacobs W. 2012. A conceptual framework for shear flow-induced erosion of soft cohesive sediment beds. *Journal of Geophysical Research* **117**: C10020. doi:10.1029/2012JC008072.

Zaimes GN, Schultz RC. 2015. Riparian land-use impacts on bank erosion and deposition of an incised stream in north-central Iowa, USA. *Catena* **125**: 61-73.

Zhu JC, Gantzer CJ, Peyton RL, Alberts EE, Anderson SH. 1995. Simulated small-channel bed scour and head cut erosion rates compared. *Soil Science Society of America Journal* **59**(1): 211-218.

Tables

Table 1. Comparison of observed bank retreat lengths and rates for the PEEPs and Pins

	Retreat Length and Rates				
Location	PEEP (cm)	PEEP (cm/s)	Pin (cm)	Pin (cm/s)	%difference
Crest*	28	1.39×10^{-4}	21	1.02×10^{-4}	27
UpperMid*	15	6.37×10^{-5}	12	5.17×10^{-5}	19
Lower Mid*	8.2	2.74×10^{-5}	6.2	2.07×10^{-5}	24
Toe*	0	0.00	12	2.45×10^{-5}	n/a

*The period for the pin measurements are only from July 1 to September 30, 2009, when the pins were installed.

Table 2. Possible sources of error between the PEEPs and Pins

Vegetation	Turbidity	Compaction	Flow	Exposure
Present throughout monitoring period but accounted for with Figure A1 (n/a)	More sand in transport, so less dirtying of PEEPs (n/a)	Less compacted soils due to flood deposits, so more possibility for spin (+)	More sustained higher flows, longer opportunities for spinning (+)	Higher overall exposure lengths, so PEEPs experience more drag (+)

Plus signs (+) indicate an enhanced PEEP retreat length; minus signs indicate a decreased retreat length; (n/a) means no net effect.

Table 3. Erodibility parameters

Event	Integrated Erosion Length (cm)	ΔT (hr)	M_{mf} (kg/s)
June 19, 2009	9.4	0.50	0.332
July 10, 2009	1.2	0.25	0.073
August 27, 2009	3.9	0.63	0.095
October 22, 2009	0.14	0.50	0.005
October 29, 2009	0.83	0.38	0.034

Table 4. Evaluation of curve fits to erosion rate vs. applied shear stress plot

Method	R^2 value	p-value	RMSE
Single-line Linear	0.37	3.78×10^{-5}	0.0198
Piecewise Linear	0.81	2.40×10^{-10}	0.0145
Single-line; Non-linear	0.52	3.75×10^{-8}	0.0281

Figure 01

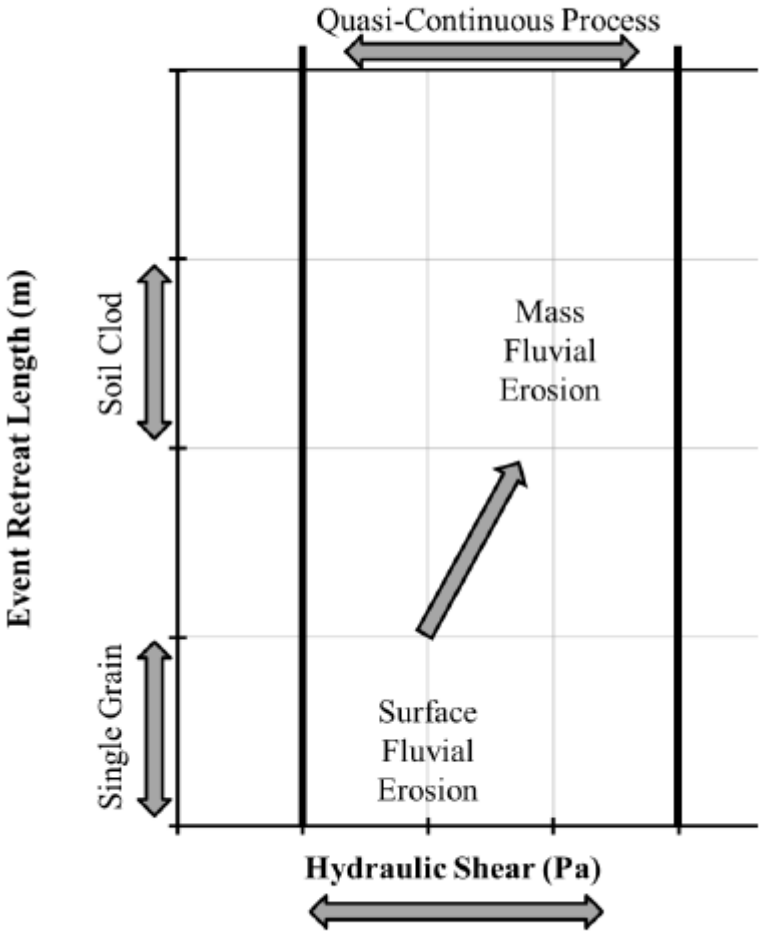

Figure 01. Conceptual representation of the different regimes of fluvial erosion (surface and mass) in terms of applied hydraulic shear stress and event retreat length.

Figure 02

Figure 02. The Clear Creek, IA watershed. (a) Monitoring location near the mouth of Clear Creek. (b) Other images of the site showing sand deposition on the bank face.

Figure 03

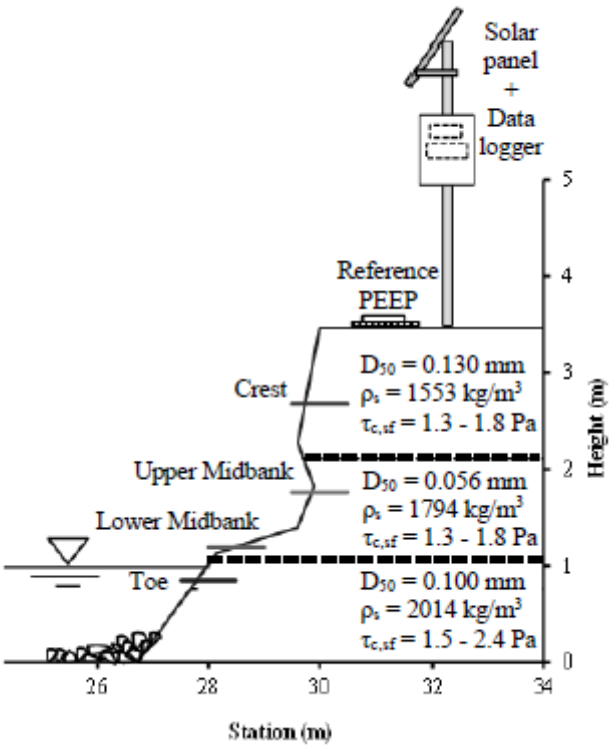

Figure 03. Schematic of the PEEP installation at the monitoring site with geotechnical properties for each bank layer (from Sutarto *et al*., 2014).

Figure 04

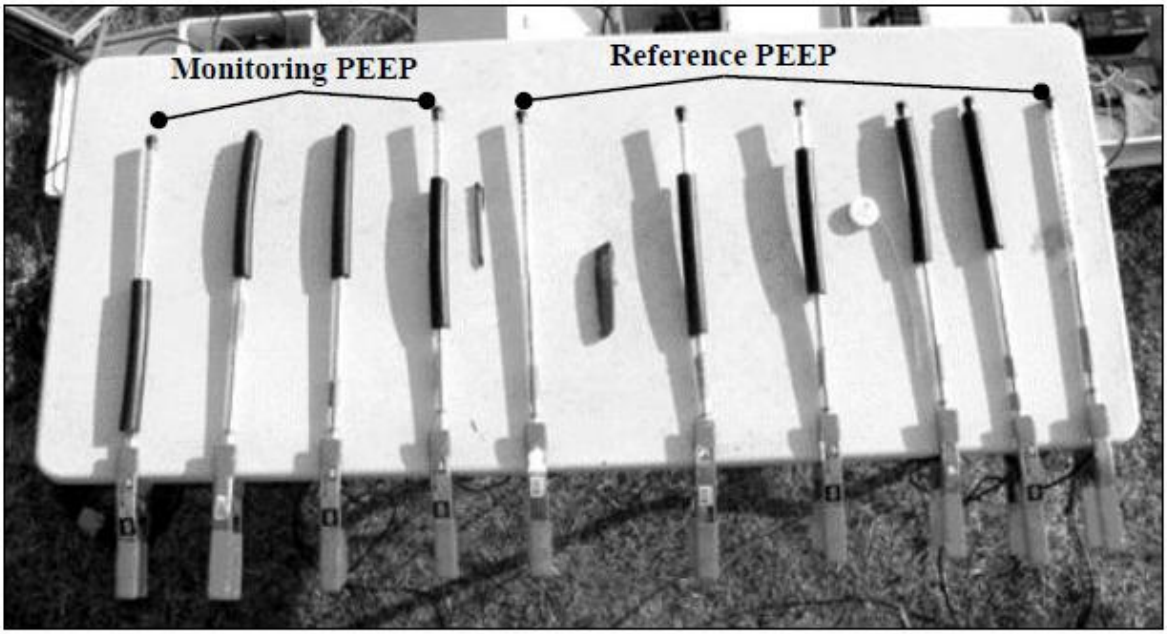

Figure 04. PEEP calibration. PEEPs were placed on a level table on the floodplain at the monitoring site. Reference PEEPs were fully exposed throughout the calibration. Black, light-tight sleeves were used to cover all diodes of the monitoring PEEPs. The sleeves were then gradually pulled back with known distances to mimic bank retreat.

Figure 05

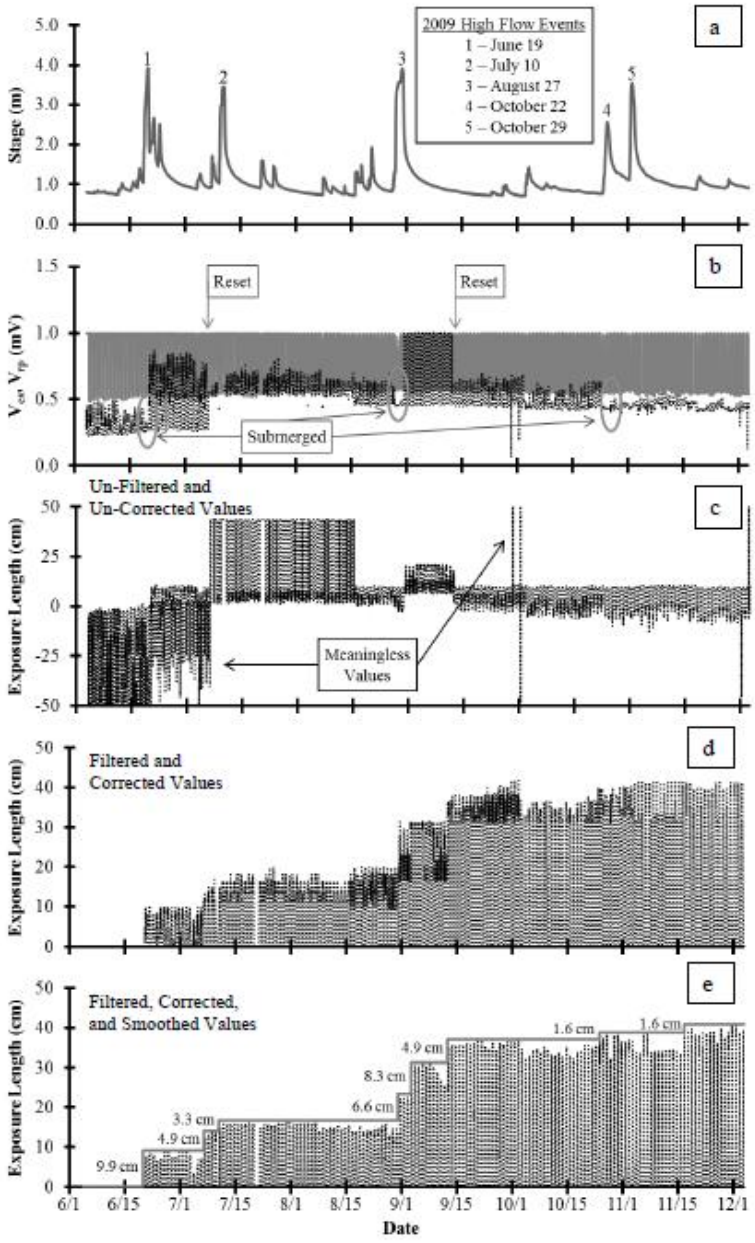

Figure 05. (a) Time series of stage between June and December 2009. (b) Time series of voltages from the monitoring PEEP at the crest, V_{cs}, shown with the dashed black line, and reference PEEP voltages, V_{rp}, shown with the solid grey line. The circles highlight drops in V_{cs} related to PEEP submergence and/or high turbidity in Clear Creek. The boxes show the times when a monitoring PEEP was reset into the bank face. (c) Time series of the un-filtered, un-corrected, and un-smoothed exposure lengths for the crest PEEP after using Eq. 1. (d) Time series of exposure lengths for the crest PEEP following the filtering and correcting stages identified in Figure A1. (e) Time series of the exposure length (black dashed line) for the crest PEEP with an 8-hour moving-averaged applied to it. The stair-cased solid line shows the estimated retreat length following the smoothing stage identified in Figure A1.

Figure 06

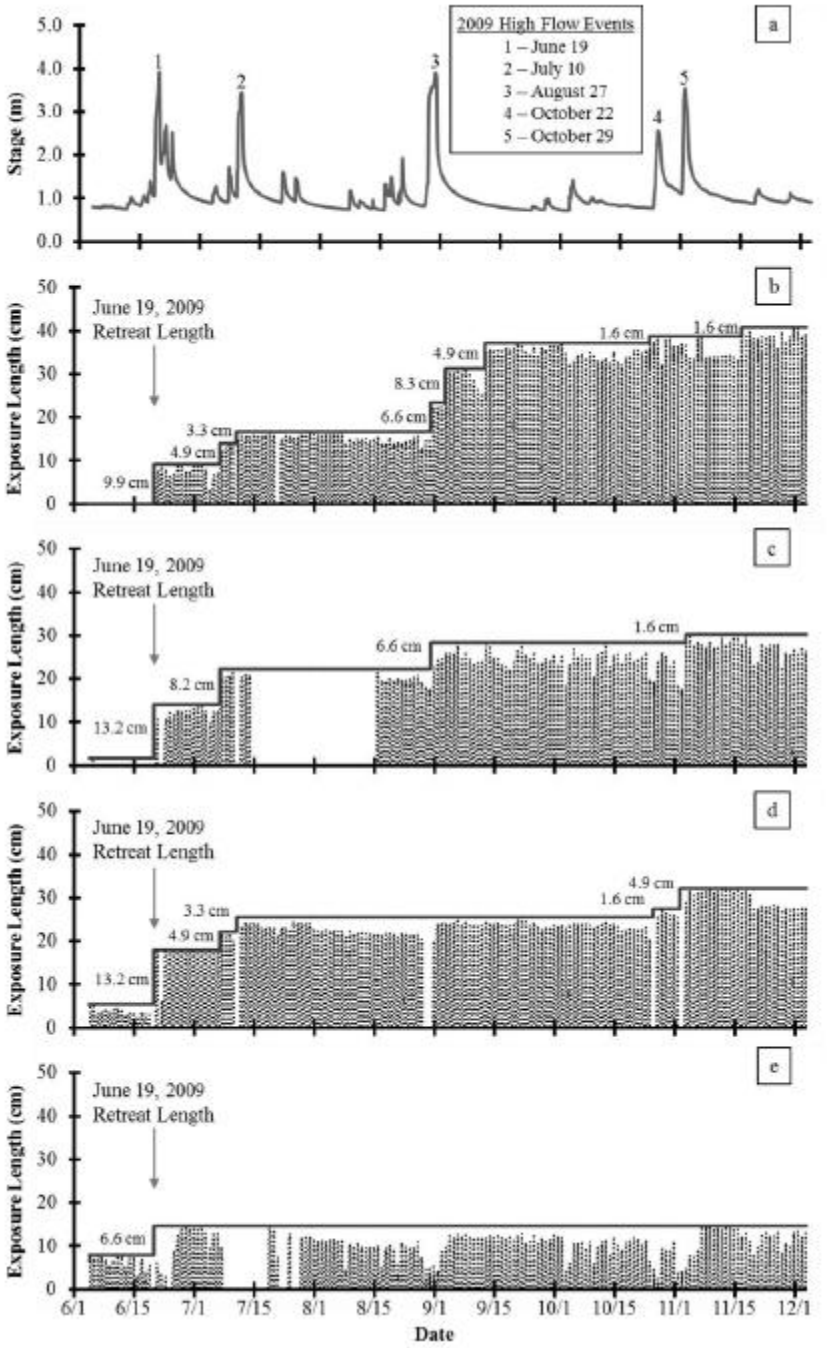

Figure 06. (a) Time series of water stage June to December 2009. Time series of the smoothed exposure lengths for the PEEPs at the (b) crest, (c) upper midbank, (d) lower midbank, and (e) toe, shown with the dashed lines. The stair-cased solid grey lines show the estimated retreat lengths following the procedure in Figure A1.

Figure 07

Figure 07. Close-up picture of the bank soil at the monitoring site in Clear Creek, which highlights the cementation at the site.

Figure 08

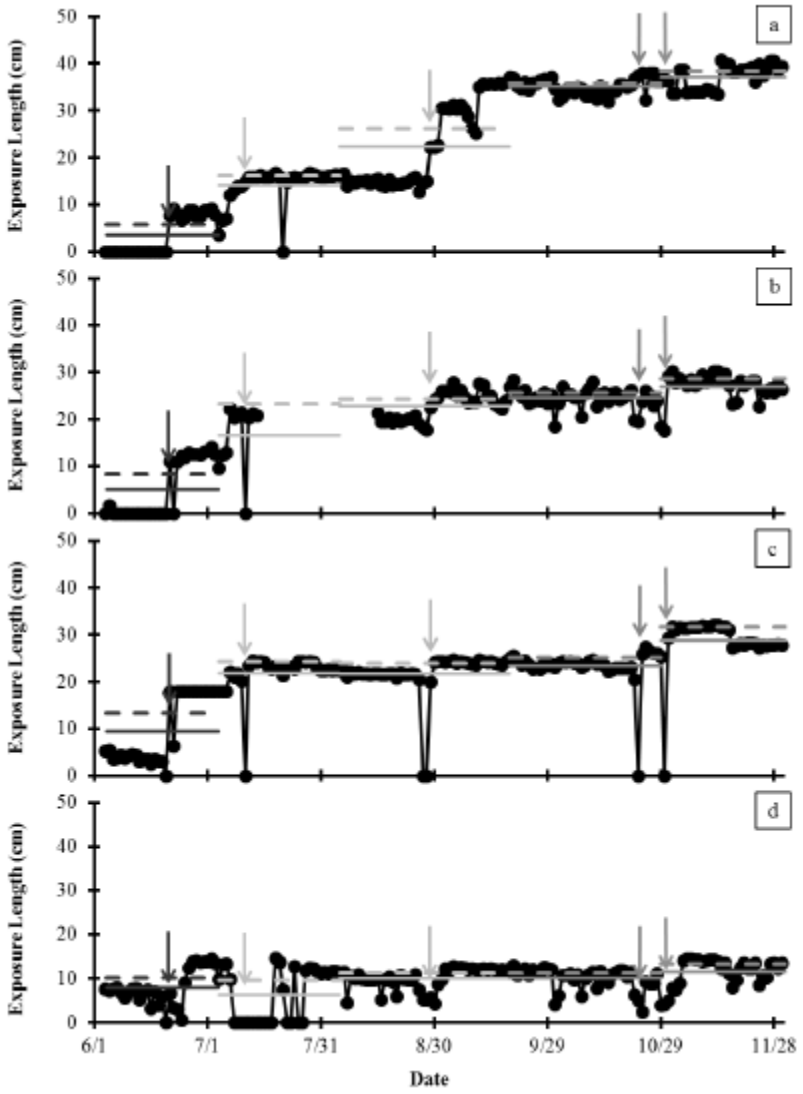

Figure 08. Shewhart control charts for the smoothed exposure lengths for the PEEP at the (a) crest, (b) upper midbank, (c) lower midbank, and (d) toe (black lines) along with the median values (solid grey lines) and the upper and lower control limit (dashed grey lines). The different greyscale represent the five runoff events capable of producing mass fluvial erosion.

Figure 09

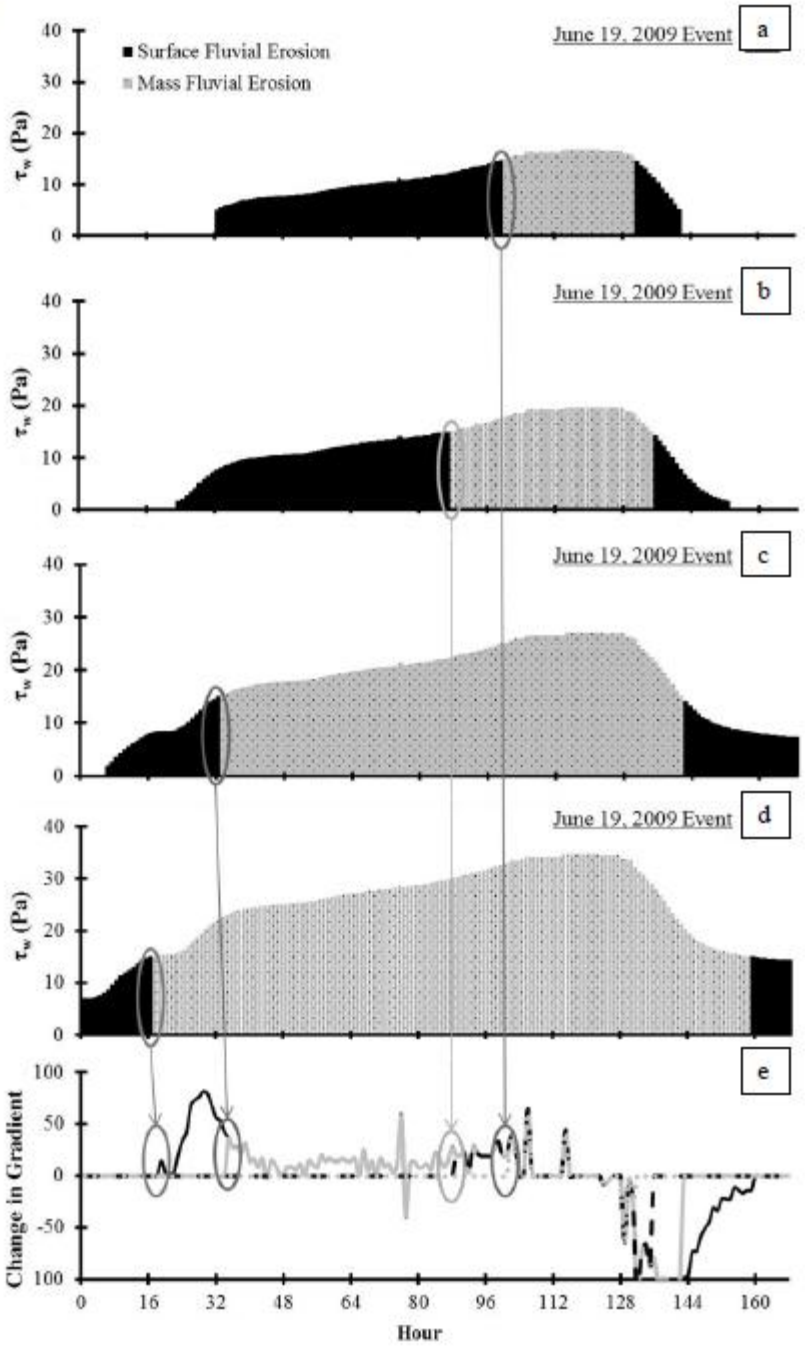

Figure 09. Determination of the time of occurrence for mass fluvial erosion (ΔT). Time series of the period when τ_w was greater than $\tau_{c,mf}$ (as seen with the dashed grey lines) for the PEEPs at the (a) crest, (b) upper midbank, (c) lower midbank, and (d) toe for the June 19, 2009 event. (e) The ΔT was determined based on the change in gradient of the time series of near bank shear stress. The change in gradient was determined as the "change in τ_w between two consecutive time intervals" divided by the "change in time between two intervals" to give the "change in gradient" of the τ_w time series.

Figure 10

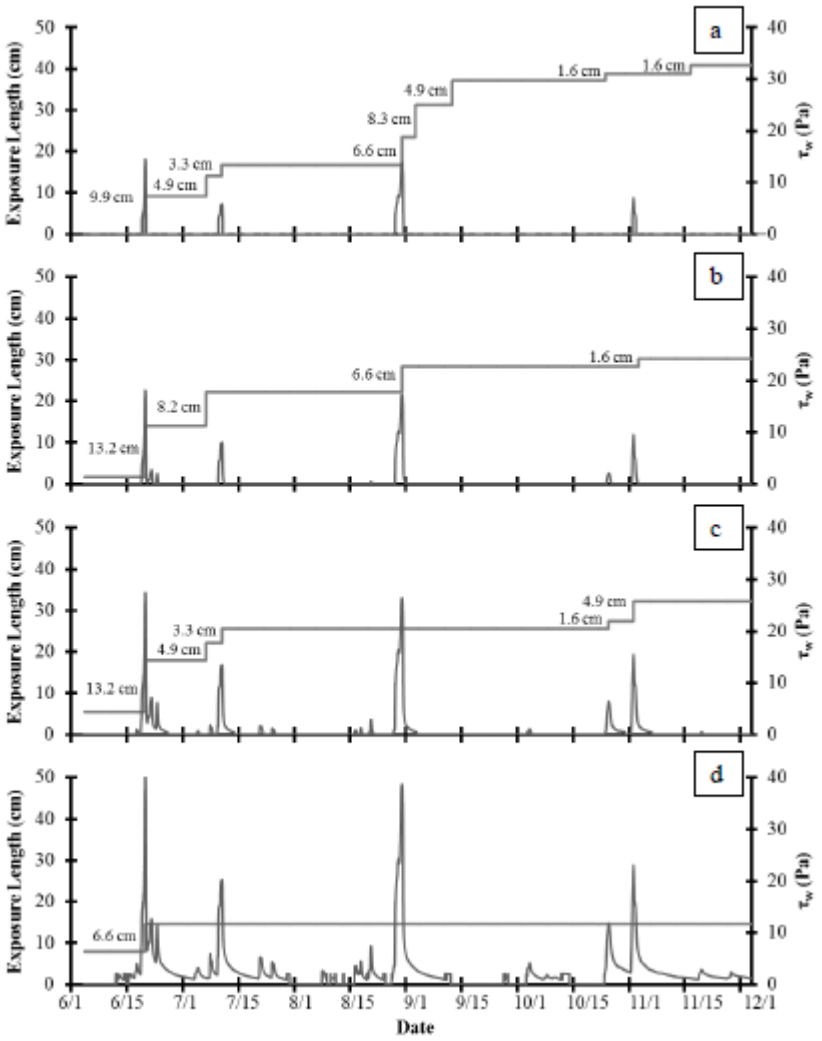

Figure 10. Time series of estimated ΔL and applied shear stresses for the (a) crest, (b) upper midbank, (c) lower midbank, and (d) toe.

Figure 11

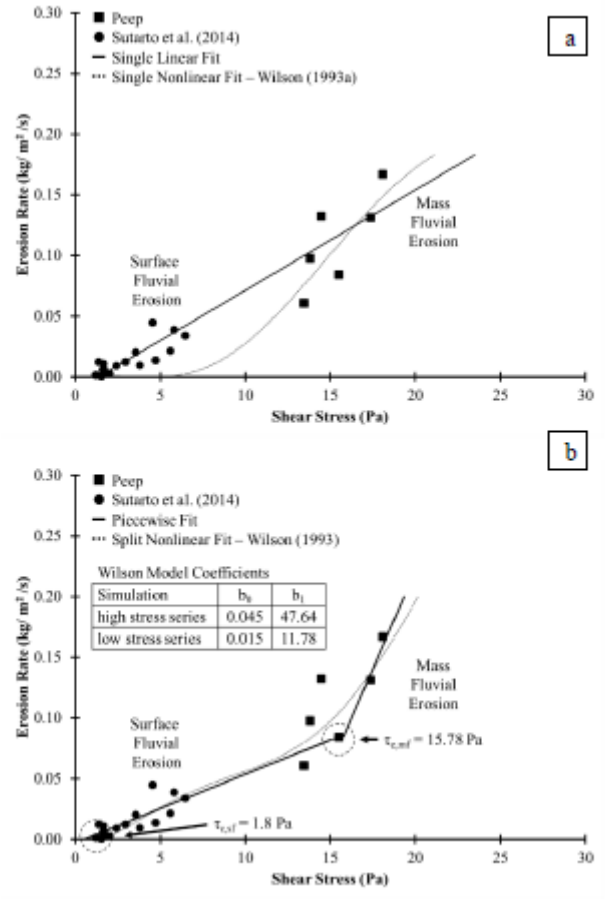

Figure 11. Surface and mass fluvial erosion regimes. (a) The data obtained from Sutarto *et al*. (2014) are in the closed black circles and from the present study are in the closed black squares. Both a single linear fit (soild black line) and a single non-linear fit (dashed black line) are plotted against the measured data to show there lack of correspondence. (b) The measured data are plotted again, but this time with a piecewise linear regression (soild black line) and a split non-linear fit (dashed black line) from Wilson (1993a,b). The mass fluvial erosional strength, $\tau_{c,mf}$, is determined as the breakpoint between the fitted solid black lines of the data obtained from Sutarto *et al*. (2014) and the present study using a piecewise regression. The split non-linear fit using the Wilson (1993a,b) detachment model and different coefficients (b_0 and b_1) for the low stress series and the high stress series.

Appendix 1

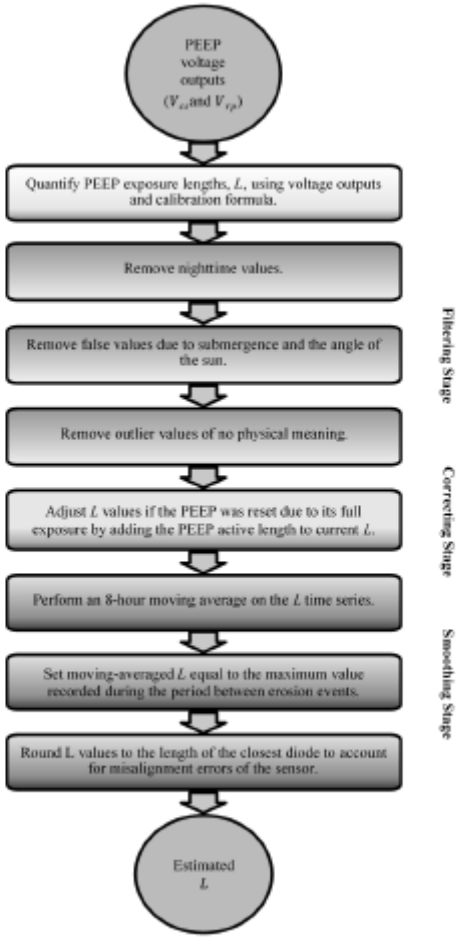

Figure A1. Procedure for estimating PEEP exposure lengths.